ARIZONA STATE UNIVERSITY Grant No. DE-FG07-02ER63505

ASU PI: James A. Tyburczy, (480) 965-2637, jim.tyburczy@asu.edu

FINAL PROGRESS REPORT: 9/2002 - 9/2005

Project ID # 86984 Project Title: **Caustic Waste-Soil Weathering Reactions and Their Impacts on Trace Contaminant Migration and Sequestration**

Lead Principal Investigator: Dr. Jon Chorover, Department of Soil, Water and Environmental Science, 429 Shantz Building, University of Arizona, AZ 85721: Tel: (520) 626-5635; Email: chorover@cals.arizona.edu

Co-Investigators: Dr. Karl T. Mueller, Department of Chemistry, 152 Davey Laboratory, The Pennsylvania State University, University Park, PA 16802; Tel: (814) 863-8674; Email: ktm2@psu.edu; Dr. Peggy O'Day, School of Natural Sciences, University of California, Merced, CA 95344; Tel: (209) 724-4338; Fax: (209) 724-2912; E-mail: poday@ucmerced.edu; Mr. R. Jeff Serne, Pacific Northwest National Laboratory, Applied Geology & Geochemistry Group, Richland, WA 99352; Tel: (509) 376-8429; Email: jeff.serne@pnl.gov *Graduate Students*: Garry Crosson, Geoffrey Bowers, Nelson Rivera, Jason Field. *Postdoctoral Scholar*: Sunkyung Choi, Wooyong Um Project: 86984

1. Introduction.

The principal goal of this project is to assess the molecular nature and stability of radionuclide (^{137}Cs, ^{90}Sr, and ^{129}I) immobilization during weathering reactions in bulk Hanford sediments and their high surface area clay mineral constituents. We focus on the unique aqueous geochemical conditions that are representative of tank waste-impacted locations in the Hanford site vadose zone: high ionic strength (*I*), high pH and high dissolved Al concentrations. The specific objectives of the work are to (i) measure the coupling of clay mineral weathering and contaminant uptake kinetics; (ii) determine the molecular structure of contaminant binding sites and their change with weathering time during and after exposure to synthetic tank waste leachate (STWL); (iii) establish the stability of neoformed weathering products and their sequestered contaminants upon exposure of the solids to more "natural" soil solutions (i.e., after removal of the caustic waste source); and (iv) integrate macroscopic, microscopic and spectroscopic data to distinguish labile from non-labile contaminant binding environments, including their dependence on system composition and weathering time. During this funding period, we have completed a large set of bench-scale collaborative experiments that integrated macroscopic observations with molecular and microscale characterizations. Although data analysis is still in process, these studies show the importance of mineral-tank waste reaction on contaminant sequestration/stabilization and aging that will control subsequent rates of desorption or dissolution after removal of the waste source.

2. Summary of Results.

Studies of the reactivity of radionuclides (Cs, Sr, I) in STWL with model clays and natural sediments were conducted by coupling macroscopic sorption-desorption experiments with spectroscopic and microscopic investigations over a wide range of reaction times. Three experimental systems were studied: (1) model clay minerals, (2) products of homogeneous precipitation from STWL, and (3) representative Hanford sediments, with (1) and (3) reacted with STWL from 1 h to 369 d. The clay minerals included illite, vermiculite, smectite and kaolinite, which constitute a sequence of micaceous weathering products with variable reactivity toward Cs^+, Sr^{2+} and I^-. Coarse and fine sediments collected from the Hanford formation (HC and HF, respectively) and Ringold Silt (RS) were studied in batch experiments and Warden silt loam was used in batch and column experiments. Solutions were analyzed by inductively coupled plasma-mass spectrometry (ICP-MS). Solid products (referred to here as "secondary phases" relative to the initial reactant minerals) were analyzed for time-dependent changes in mineralogy and modes of contaminant bonding by a variety of methods, including X-ray diffraction (XRD), scanning and transmission electron microscopy (SEM and TEM) with energy dispersive

spectrometry (EDS), thermogravimetric analysis (TGA), nuclear magnetic resonance (NMR), X-ray absorption spectroscopy (XAS), including extended X-ray absorption fine structure (EXAFS) and X-ray absorption near-edge structure (XANES) analysis, and Fourier-transform infrared spectroscopy (FTIR).

Clay Mineral Systems

Specimen clay minerals were reacted in batch aqueous systems of a synthetic tank waste leachate containing Cs^{+} and Sr^{2+}, where both metals were present as co-contaminants at initial aqueous concentrations from 10^{-5} to 10^{-3} M (all at 298 K). The reactant clays were the 2:1 layer-type silicates illite (Il), vermiculite (Vm) and montmorillonite (Mt), and a 1:1 layer-type kaolinite (Kt). At specified intervals from 1 h to 369 d, samples were removed for multifaceted analysis of "dissolved" (< 0.2 μm), "colloidal" (0.2-2 μm) and "solid phase" (> 2 μm) constituents. The type of initial clay affected the rates of (i) hydroxide promoted dissolution of Si, Al and Fe, (ii) precipitation of secondary solids, and (iii) uptake and extractability of Cs and Sr (Chorover et al., 2003; Choi et al., 2005a). Initial Si release to solution followed the order Mt~Kt > Vm > Il. An abrupt decrease in soluble Si and/or Al after 7 to 33 d for Kt, Mt and Vm systems, and after 190 d for Il suspensions, was concurrent with accumulation of secondary aluminosilicate precipitates. Precipitation resulted in significant removal of STWL Al from solution when parent mineral dissolution was rapid, as was observed for Mt and Kt. Importantly, we found that Cs and Sr contaminant concentrations themselves had a strong negative impact on clay mineral dissolution rates, neophase precipitation rates, and the structural order of secondary precipitates. This, in part, motivated a separate set of studies on homogeneous nucleation to examine the impacts of contaminant concentration in the absence of reactant solids. Strontium uptake exceeded that of Cs in both rate and extent, although sorbed Cs was generally more recalcitrant to subsequent desorption and dissolution. After 369 d, reacted Il, Vm, Mt and Kt solids retained up to 25, 46, 20 and 16 mmol kg^{-1} of Cs. The fraction of sorbed Cs that was not removed in subsequent ion (Mg^{2+}) exchange or oxalic acid (AAO) dissolution reactions amounted to 70% for Il, 100% for Vm, 20% for Mt and 63% for Kt of the total sorbed mass, indicating a significant pool of strongly retained (or recalcitrant) Cs in all clay mineral systems. After 369 d of reaction time, the same solids sorbed 33 (Il), 47 (Vm), 38 (Mt) and 45 (Kt) mmol kg^{-1} of Sr, of which 0% (Il), 57% (Vm), 58% (Mt) and 87% (Kt) was non-extractable (Chorover et al., 2003; Choi et al., 2005a).

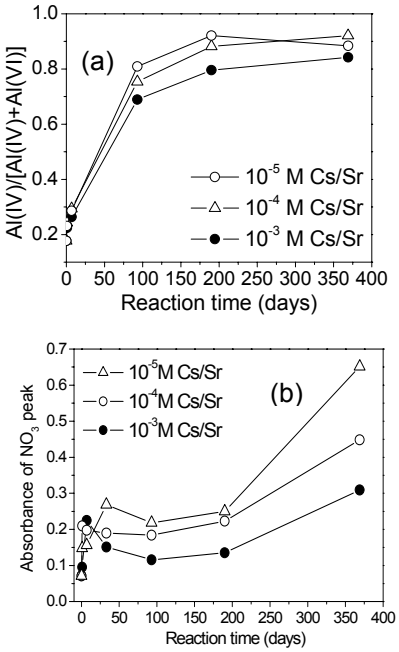

Figure 1. Spectroscopic monitoring of reaction progress in Mt systems. (a) Ratio of tetrahedral to total Al in ^{27}Al MAS NMR spectra provides a quantitative measure of zeolite formation. (b) Infrared absorption bands in DRIFT spectra show accumulation of structural NO_3 in product solids.

Solid Phase Characterizations

XRD, FTIR & SEM/TEM: Extensive microscale analyses (Choi et al., 2005b) indicated that incongruent clay dissolution resulted in an accumulation of secondary aluminosilicate precipitates identified as nitrate-sodalite, nitrate-cancrinite, chabazite and zeolite X. Contaminant fate was found to be strongly dependent on competing uptake by parent clays and weathering products. TEM-EDS results indicated that the high affinity of Cs for Il was due to adsorption at frayed edge sites. The Il system also contained Sr-rich aluminous precipitates after 369 d of reaction. In both Kt and Mt systems, Cs and Sr were co-precipitated into increasingly recalcitrant spheroidal precipitates over the course of the experiment, whereas contaminant association with Mt platelets was less prevalent. In contrast, Cs and Sr were found in association with weathered Vm particles despite the formation of spheroidal aluminosilicate precipitates that were similar in morphology to those formed from Mt or Kt dissolution. The rate of precipitation of nitrate-bearing solids could be tracked by

quantifying "fingerprint" bands in FTIR spectra (Choi et al., 2005b; Fig. 1b).

Solid-state NMR: ^{29}Si and ^{27}Al magic-angle spinning (MAS) NMR spectroscopy provided structural and kinetic information about the kaolinite and montmorillonite specimen clay systems. By performing MAS NMR experiments at a range of magnetic field strengths (facilitated by access to equipment at the Environmental Molecular Sciences Laboratory at PNNL), we have extracted full sets of relative populations, isotropic chemical shift values, and quadrupolar parameters for tetrahedrally coordinated Al sites in four new phases formed by the weathering of kaolinite in an STWL for up to 369 days (Crosson et al., submitted). The kinetics of secondary phase formation can then be mapped based on total Al speciation or the individual formation kinetics of all four phases (Fig. 2). The data indicate incipient formation of sodalite, followed by transformation to more stable cancrinite, which is consistent with XRD and TEM/SEM results, but these data also provide highly accurate quantitation. Studies of montmorillonite (Choi et al., 2005b) have provided overall quantitative rates for formation of secondary phases (Fig. 1a).

Novel double-resonance NMR methods were employed to isolate spectra deriving only from radionuclide-containing neoformed phases to extend the molecular-scale understanding of contaminant sequestration. ^{29}Si/^{133}Cs double-resonance experiments were first accomplished on a model Cs-exchanged sample of chabazite (Crosson, 2005), one of the minerals identified as a reaction product in the clay systems (Chorover et al., 2003). Both Rotational-Echo Double-Resonance (REDOR) and Transfer of Populations via Double-Resonance (TRAPDOR) experiments were successful for indirect detection of the Cs within the pores of the chabazite. Initial attempts at ^{29}Si/^{133}Cs double-resonance were also successful in studies of kaolinite after reaction for 190 days with a SWTL containing 10^{-4} M Cs and Sr (Crosson, 2005). Further studies are planned that would include ^{27}Al/^{133}Cs double-resonance as well as ^{27}Al/^{87}Sr experiments.

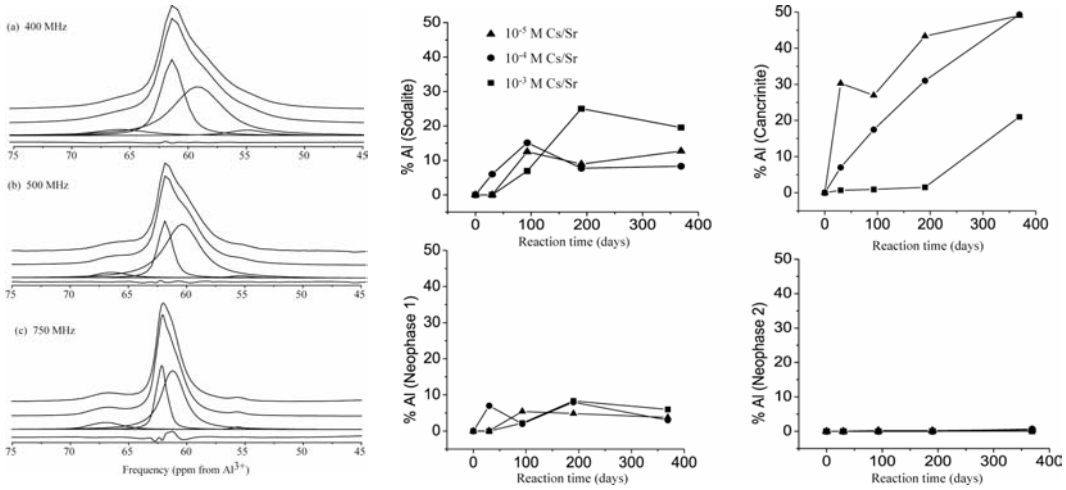

Figure 2. ^{27}Al MAS NMR acquired at three magnetic field strengths (left: top-400 MHz, middle-500 Mhz, bottom-750 MHz) provide the data for full quantification of secondary solid phase speciation for specimen kaolinite samples reacted with a STWL solution throughout the time series and as a function of Sr and Cs co-contaminant concentrations (adapted from Crosson, 2005).

Synchrotron XAS: Bulk and microfocused Sr K-edge EXAFS was used to elucidate Sr coordination in reacted kaolinite samples. Bulk EXAFS (mm-sized beam) of a homogeneous sample provides a view of the Sr bonding environment averaged over all molecular sites in the sample, while microfocused EXAFS (~15-30 μm diameter beam) gives particle-specific coordination. Individual particles (~2-5 μm in diameter) were dispersed and imaged with SEM prior to the synchrotron run. A beam size larger than the particle size was used to increase beam-sample stability. X-ray element maps were made prior to EXAFS data collection in order to insure that spectra were collected only from isolated, Sr-bearing particles and

not from multiple particles. These data (Choi et al., submitted) are the first Sr K edge micro-EXAFS spectra collected on natural geomedia.

Fits of bulk kaolinite EXAFS spectra showed distinct changes as a function of reaction time (Choi et al., submitted). Quantitative analysis of samples reacted for 1 and 7 d showed that the average local atomic structure around Sr is similar to the local structure of crystalline $SrCO_3$, which was not detected by XRD or SEM. This result may imply a small particle size for the $SrCO_3$ precipitate, a surface coating, or a small amount of $SrCO_3$ that is below detection with XRD. Although CO_2 was excluded from the reactant solutions, diffusion of ambient CO_2 into the samples during the experiments was sufficient to exceed the solubility of $SrCO_3$(s). The EXAFS spectrum at 33 d had few features beyond the first oxygen coordination shell around Sr. Lack of second-neighbor backscattering atoms may indicate that Sr is present primarily as a hydrated species, or may result from cancellation of backscattered wave functions if Sr is bonded in several sites of different coordination. The difference between the 1 and 7 d samples and the spectrum at 33 d indicates that the $SrCO_3$ phase is transient. Samples reacted for longer than 33 d showed second-neighbor backscattering features different from those of the less reacted samples. Bulk EXAFS spectra of samples reacted for 93, 190, and 369 d, and a 369-d reacted sample subjected to AAO extraction (which is intended to remove poorly crystalline solids), all showed similar spectral features. Quantitative fits indicate that Sr is associated mainly with zeolite or feldspathoid phases. X-ray diffractograms of these samples (Chorover et al., 2003) showed the emergence of new peaks, beginning at 93 days, attributable to the zeolite Al-chabazite or the feldspathoids sodalite and cancrinite. A second-neighbor peak at ~3.4-3.5 Å is consistent with Sr incorporation into one or more of these phases and partial dehydration and bonding of Sr to framework O atoms at a cation site, giving rise to scattering from Al or Si atoms at these characteristic interatomic distances. Chemical extractions of 93-d to 1-yr samples showed that most sorbed Sr (70-80%) is associated with non-extractable phases (i.e., unrecovered in the extraction by mass balance) (Chorover et al., 2003).

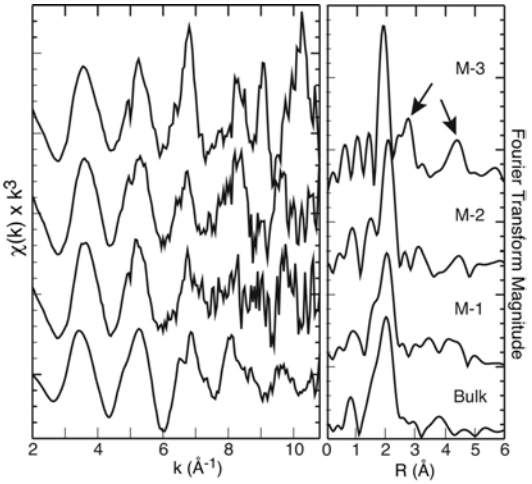

Figure 3. Microfocused and bulk Sr K-edge EXAFS of kaolinite reacted with STWL for 33 d. Spectra from 3 different particles (M-1, M-2, M-3) are compared to the bulk sample spectrum; particle M-3 shows strong backscattering features at high k (arrows) that indicate close second-neighbor atoms.

The 33-d bulk kaolinite sample showed no analyzable features at atomic distances greater than the first O coordination shell in bulk EXAFS. Likewise, XRD showed no evidence of zeolite, feldspathoid, or carbonate phases. Imaging with SEM and TEM, however, revealed the presence of morphologically distinct particles with relatively high concentrations of Sr. Microfocused EXAFS was collected from three individual particles in this sample. Although data quality is generally poorer in microfocused mode, differences in backscattering features are apparent among the three spectra (Fig. 3). Two of the spectra showed no or weak backscattering beyond the first O coordination shell. This can be interpreted as a predominance of Sr environments where Sr atoms are primarily coordinated by water or hydroxyl ligands. A third spectrum showed strong backscattering features at distances beyond the first atomic shell. At least two sets of second-neighbor atoms are present, one between ~3.3-3.5 Å and a second at ~4-5 Å from a central Sr (Fig. 3). Scattering at the longer inter-atomic distances can only come from high Z atoms (scattering from low Z atoms is typically too weak at such distances at room temperature). Least-squares fits assuming Sr coordination in zeolite and feldspathoid phases indicates two different sets of Al or Si atoms at ~3.3 and 3.5 Å, which requires partially dehydrated Sr at cation sites in the framework structure. Backscattering from 4-5 Å in this spectrum is consistent with the presence of Sr and/or Cs atoms in adjacent cation sites within a zeolite channel or in an adjacent channel.

The bulk EXAFS spectrum, which showed no strong second-neighbor backscattering, suggests that hydrated Sr is dominant over dehydrated Sr on average at 33 d. However, SEM/EDS analyses indicated that most Sr is strongly associated with distinct particles and not randomly distributed on all phases. In addition, stepwise chemical extractions showed pools of exchangeable, AAO-extractable, and strongly bound Sr and Cs at 33 d (Chorover et al., 2003). *These data are consistent with the EXAFS interpretation of both hydrated and dehydrated Sr bonded to different cation sites in newly formed zeolite or feldspathoid phases.*

Collectively, the clay mineral data document a complex time-dependent interplay between mineral transformation and contaminant partitioning in incongruently weathering systems [26,27,28,29]. These model studies indicate that parent mineralogy plays a central role in controlling (i) the rate and extent of Cs and Sr sequestration into recalcitrant forms and (ii) the influence of contaminant concentration on mineral transformation rates. The extent to which contaminants are sequestered by neoformed precipitates depends on sorptive affinity for the parent clay and clay dissolution rate. In systems with carbonate present and sufficient Sr, the EXAFS data suggests that Sr may form a transient carbonate phase at alkaline pH, as seen in previous studies of Sr adsorption on kaolinite and oxide phases [122]. In the case of kaolinite and montmorillonite, rapid dissolution and relatively low concentrations of high-energy sorption sites for Cs and Sr result in the long-term uptake of these contaminants into product zeolites that form on time scales of weeks to years. Since the rate of clay dissolution at high pH is surface-reaction limited, increased contaminant concentrations and associated sorption of Sr (and possibly Cs) to reactive surface sites apparently reduces the rate of OH^- attack, diminishes the release of Si to solution, and slows the formation of zeolite/feldspathoid products. Bulk chemistry and NMR results from homogeneous nucleation studies (see below) and clay experiments indicate the importance of Si/Al solution ratio in determining the feldspathoid or zeolite products. The combination of hydrated and dehydrated Sr in the reaction products of kaolinite at 33 d shows a kinetic limitation to the transition from weakly bound, hydrated Sr to more strongly bound dehydrated Sr associated with product phases. At longer reaction times, Sr is primarily dehydrated and non-extractable, and appears to be strongly bound at cation sites in zeolite/feldspathoid phases. In the case of illite and vermiculite, high affinity bonding to the parent clay, even in the presence of STWL, and slower dissolution rate diminishes the accumulation of Cs in neoformed zeolites in those systems (Choi et al., 2005a).

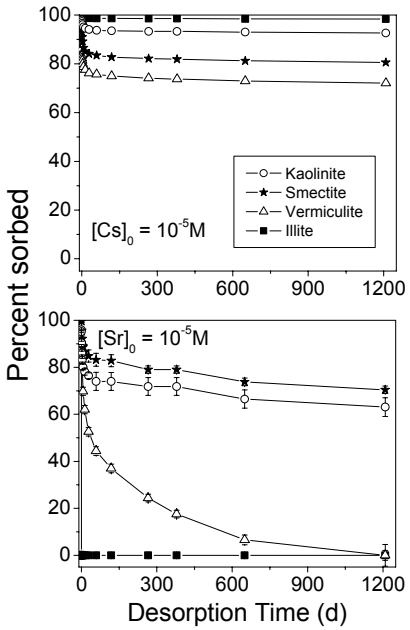

Figure 4. Desorption kinetics of Cs and Sr from reacted clays following 10 months of reaction with STWL at initial Cs and Sr concentrations = 10^{-3} M. Initial values of "% sorbed" (0 days of desorption) refer to the mass fraction removed from STWL solution, which was often close to 100%. Reacted solids were immersed in contaminant-free 5 mM $CaCl_2$ solutions at pH 8 that was replenished repeatedly for over 40 months.

Dissolution Kinetics of Sr and Cs Sequestered in Reacted Clays: Contaminant sequestration into solid phase weathering products as described above has important implications for the reactive transport of these constituents in the Hanford vadose zone as the contaminated sediments come into contact with natural porewaters. The development of a predictive understanding of contaminant release from mineral solids upon removal of the caustic waste source is the primary focus of this proposal. As an initial assessment, we measured the desorption kinetics of Cs and Sr, as well as dissolution of Si, Al and Fe (not shown), from the four model clays reacted for 10 months with STWL as described above. Desorption was measured in a 5 mM $CaCl_2$ solution at pH 8 (Fig. 4). The contaminant-free

$CaCl_2$ solutions were decanted and replenished at regular intervals to prevent solution phase accumulation of Cs, Sr, Al or Si. Aside from a small initial release, the data indicate very little Cs desorption or dissolution from the reacted solids after 40 months. Although Sr is more readily re-mobilized during the desorption/dissolution reaction, we also observed a large fraction that is relatively recalcitrant to removal in systems in which significant mineral transformation has occurred (Kt and Mt). In those systems, 60-80% of the sorbed Sr mass remained immobilized in the solid phase after 40 months of reaction with simulated fresh water. Irreversible association of Cs and Sr with recalcitrant solids is evidenced by *immobilization of these contaminants in the solid phase over a desorption timeframe that exceeds the time of the uptake reaction by four times*.

C.2.3 Homogeneous Nucleation Studies

Since our prior work indicated that Si dissolution kinetics and contaminant concentrations were key factors controlling the rate and trajectory of secondary solid phase formation, batch aqueous experiments of synthetic tank wastes containing Cs, Sr, and I in the presence of dissolved Si were conducted over a range of molar ratios of Si to Al in order to characterize reaction products formed in the absence of kinetic effects that might arise from the presence of a solid. Synthetic tank waste leachate (STWL) (2.0 M Na^+, 1.0 M NO_3^-, 0.05 M $Al(OH)_4^-$, and 1.0 M OH^-) was spiked to give three initial aqueous phase Cs^+, Sr^{2+} and I^- concentrations, where individual contaminants (Cs, Sr or I) and co-contaminant mixtures (Cs/Sr. Cs/I, Sr/I and Cs/Sr/I) were added at levels of 10^{-5}, 10^{-4} or 10^{-3} M. 40 % Ludox colloid was used as a source of soluble Si (dissolved immediately upon introduction to STWL). Molar ratios of Si to Al were 1:1, 2:1, 10:1 and 20:1. Batch experiments were conducted at 25 and 60°C in sealed polypropylene copolymer (PPCO) bottles for 1 month, at which time solutions were analyzed. Reaction products were centrifuged, washed, and freeze-dried for characterization by XRD, SEM/TEM, FTIR and NMR.

Solid Phase Characterizations

XRD, SEM/TEM & FTIR: At a Si/Al ratio of 1:1, XRD showed a mixture of feldspathoid sodalite ($Na_8[AlSiO_4]_6(NO_3)_2$) and a smaller amount of cancrinite ($Na_8(Al_6Si_6O_{24})(NO_3)_2 \bullet 4H_2O$) as products. At 2:1 Si/Al, NO_3-cancrinite was the primary product. At high Si/Al ratios (20:1 and 10:1), reaction products were primarily zeolite X and amorphous phases (by XRD). There were no significant differences in mineralogy at room temperature and 60°C, and no variations with the contaminant concentration. Results from FTIR were consistent with XRD, showing typical nitrate and fingerprint bands for cancrinite-bearing samples and higher intensities for hydroxyl and water bands for high Si/Al reaction products. Likewise, TEM showed morphological differences as a function of initial Si/Al. Lath-shaped particles, which are typical of synthetic cancrinite, were observed at Si/Al of 2:1 at room temperature and 60°C. Spheroidal phases (~1 μm) with spikes on the particle edge were present at Si/Al = 1:1. At Si/Al ratios of 10:1 and 20:1, extremely fine particles of different sizes were observed that were susceptible to beam damage, suggesting hydrated or unstable phases.

Solid-State NMR: The homogeneous nucleation products were studied by ^{27}Al MAS NMR performed at three field strengths (7.0 T and 9.4 T at Penn State, and 17.6 T at the PNNL High-Field Magnetic Resonance Facility). In each case, the spectra show only tetrahedrally coordinated Al species in the precipitated phases and an increasing number of precipitated species as the Si/Al ratio of the parent solution decreased. High-resolution measurements made at 17.6 T demonstrate that the 20:1 Si/Al precipitates contained only a single tetrahedral Al peak (60.2 ± 0.5 ppm), while four distinct resonances were observed in the tetrahedral region for the 2:1 and 1:1 Si/Al samples. From analysis of multiple field data, little change in quadrupolar product (P_q) or isotropic shift was observed as a function of contaminant ion concentration, but slight variations in the chemical shift were observed as the contaminant varied from Cs to Sr to I. Quantitative ^{27}Al measurements showed that the ratio of the four precipitated phases varies as a function of the parent solution Si/Al ratio.

Silicon (^{29}Si) MAS NMR measurements were made on the same samples at 7.0 T. At high Si/Al in solution, multiple Si peaks were observed in the precipitates, with spacings indicative of Si tetrahedra with varying numbers of nearest neighbor Al tetrahedra. Five peaks were clearly resolved in the 20:1

Si/Al samples and the Si/Al ratio of the precipitate phase was calculated to be 1.48 ± 0.03. Aluminum spectra of the 10:1 Si/Al precipitates indicate that two phases are present in this system. In precipitates from parent solutions of low Si/Al, a single Si peak was present at a shift indicative of Si tetrahedra with four nearest neighbor Al tetrahedra. Measurements were also made on solids formed at 60 °C from 2:1 and 1:1 solutions. Only minor variations in peak shift were observed in the Al spectra between the two temperatures, and no discernable difference was apparent in the silicon spectra. These data support the conclusion that zeolite-type or other fully tetrahedral aluminosilicate phases are produced in STWL weathering environments, and that the homogeneous reaction product depends more strongly on the Si/Al ratio than on temperature (up to 60°C) or concentration of the contaminant species. Precipitation studies are currently underway with molar Si/Al ratios down to 0.05 to cover the full range observed in heterogeneous experiments. *Although data analysis is still in process, results suggest that the effect of contaminant concentration on dissolution and mineral transformation observed in heterogeneous experiments results from sorptive interactions with parent minerals.*

C.2.4 Hanford Sediments

Contaminant weathering studies on the Hanford sediments (Hanford Coarse-HC, Hanford Fine-HF, and Ringold Silt-RS) were conducted in a manner identical to those described above for the model clay systems. These data indicated similarities but also important differences with the clay experiments (Chorover et al., 2004; Chorover et al., submitted). Rates of Si dissolution and re-precipitation with Al followed the order RS > HC > HF. SEM images revealed weathered surfaces of primary minerals (feldspars, quartz and illite) and the formation of crystalline secondary solid phases (including nitrate-cancrinite) after reaction for 183 d, which were confirmed by XRD. The precipitation of nitrate-bearing secondary minerals was quantified by time-dependent increases in infrared NO_3 stretching absorbances (*ca*. 1400 cm^{-1}) in DRIFT spectra of washed solids. At early reaction times, sorbent affinity (mass basis) for Cs and Sr decreased in the order RS > HF > HC; however, all sediments had similar Sr sorption capacities after several months of reaction. Strontium uptake exceeded that of Cs for nearly all sediments and reaction times. After 374 d, the total amount of Cs and Sr sorbed in all systems ranged from 15-37% and 80-93% of the initial concentrations, respectively. Although time-dependent trends for Cs uptake were not clearly evident, the fraction of residual Cs increased slightly over time despite fluctuations. Strontium became progressively recalcitrant to desorption after 92 d, suggesting a significant role for Sr co-precipitation, as was observed for the clay mineral systems (Chorover et al., submitted).

Bulk Sr K-edge EXAFS spectra of sediments reacted for 369 d were collected by the methods described above for clay minerals. The EXAFS spectra of all three reacted sediments are similar, but subtle variations in beat patterns and Fourier transforms indicate differences in local atomic structure around Sr (Fig. 5). In general, all of the spectra have similarities to the spectrum of $SrCO_3$(s) and initial fits indicate second-neighbor Sr backscatterers at distances consistent with this local structure. This analysis suggests at least one Sr component that is associated with a carbonate phase. Some of the spectral features, however, have similarities to Sr associated with zeolite phases, which is particularly notable in the RS spectrum. This observation suggests the presence of a second Sr component associated with zeolite or

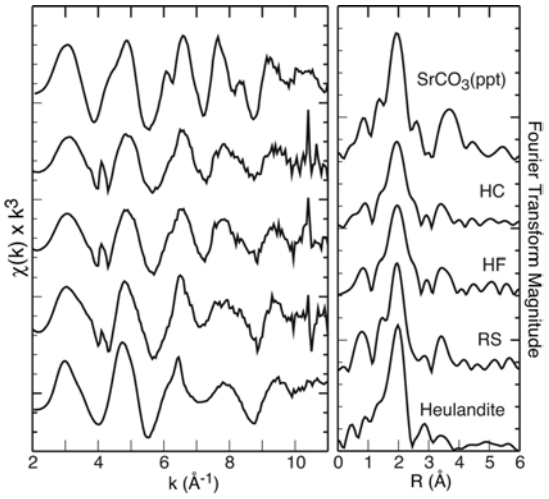

Figure 5. Room temperature Sr K-edge EXAFS of Hanford sediments (HC, HF, and RS) compared to two reference compounds, freshly precipitated $SrCO_3$(ppt) and a natural Sr-bearing heulandite ($SrCO_3$ and heulandite spectra from O'Day et al., 2000).

aluminosilicate phases, probably as dehydrated Sr as discussed above which gives rise to backscattering from second-neighbor Al or Si atoms. Analysis is underway to quantify these relative fractions. *These preliminary data suggest that, in natural sediments containing pedogenic carbonate and clay minerals, reaction with tank waste may lead to formation of new carbonate and aluminosilicate minerals that compete for uptake of Sr and Cs.* Desorption of Cs and Sr from sediments weathered in STWL for 10 months was measured at pH 8 in both 10 mM KCl and 5 mM $CaCl_2$ solutions. Initial desorption rates of both contaminants increase with increasing sorbed mass (Fig. 6, note rates are plotted on log scale). Kinetic release data for the two contaminants are quite different. Whereas Cs release is accelerated by reaction with K^+, particularly at low loadings, Sr release is enhanced in the presence of Ca^{2+} over the full sorption range. These results are consistent with Cs sorption to frayed edge sites of micaceous minerals at low initial contaminant concentrations (exchangeable only with a cation of similar hydration enthalpy and size), and sorption to low affinity sites at higher concentrations (also see McKinley et al. 2001 ; Zachara et al. 2002). For Sr, desorption is much more effective in the presence of Ca^{2+}, also suggesting the potential for Sr exchange in zeolite and/or carbonate sites as suggested by the EXAFS data.

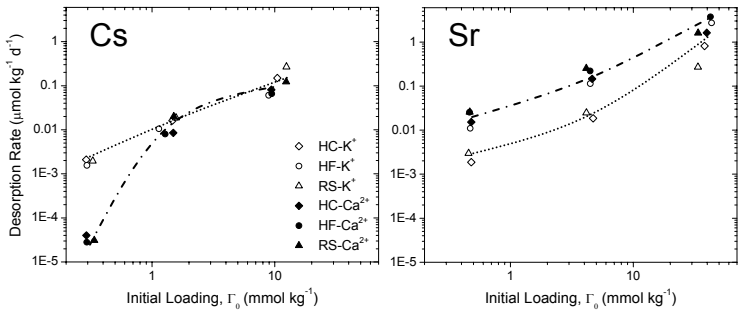

Figure 6. Rate of Cs and Sr desorption from Hanford sediments in 10 mM KCl or 5 mM $CaCl_2$ as a function of initial loading to the solid phase. Uptake from STWL occurred over a 10 month reaction period prior to desorption-dissolution experiments.

C.2.5 Solid-State Sr NMR Studies

Complimentary to EXAFS and X-ray studies, solid-state NMR of ^{87}Sr can provide details on local Sr coordination, but ^{87}Sr is a very difficult nucleus to detect via NMR for several reasons. We completed magic angle spinning (MAS) Sr NMR studies on simple crystalline compounds and showed that MAS is an effective tool for analyzing Sr nuclei in highly symmetric environments [19] . MAS rotor-synchronized echo experiments were used to calculate the distribution of electric field gradients (efgs) brought about by point defects in the crystal structures of SrO, $SrCl_2$, and SrF_2. These defects cause local variations in the electric field gradient manifested as a distribution of small quadrupolar coupling constants that can be determined by examination of the spinning sideband pattern. These data confirm that if Sr is present in a symmetric binding environment, detection and analysis will be straightforward with conventional MAS. However, MAS is difficult to apply to more complicated structures, as the large quadrupole moment of Sr produces broad resonances in the presence of any appreciable electric field gradient. MAS experiments of $Sr(NO_3)_2$ and $SrSO_4$, both of which possess quadrupolar coupling constants in excess of 10 MHz, at 9 kHz in an 11.74 T magnet have been ineffective in improving spectra. MAS NMR results from 21.14 T did show an improvement in the MAS NMR of $Sr(NO_3)_2$, but proved ineffective for larger quadrupolar coupling strengths.

We therefore have explored other means to enhance the sensitivity of low-γ quadrupolar nuclei, such as performing quadrupolar Carr-Purcell Meiboom-Gill (QCPMG) experiments [74] at the highest available external magnetic field strength. QCPMG spectra were collected for $Sr(NO_3)_2$, $SrCO_3$, and $SrSO_4$ (21.14 T NMR spectrometer at PNNL's High Field Magnetic Resonance Facility, HFMRF). The Sr sites in these materials were characterized by extracting the quadrupolar parameters (C_q and η) and isotropic chemical shift (δ_{iso}) through iterative simulations of the spectra (SIMPSON solid-state NMR simulation package). These parameters are highly sensitive to local symmetry and electronic structure about the Sr nuclei and therefore provide information related to coordination, bonding, and the identity of neighboring atoms. As expected, there was a substantial improvement in the sensitivity of ^{87}Sr NMR

measurements made at 21.14 T (Bowers and Mueller, 2005). *Improvements in spectral signal-to-noise from the QCPMG sequence results in up to ten thousand-fold reductions in experiment time, demonstrating that QCPMG is a promising method for studying Sr resonances in clays and zeolites.* The Mueller group is scheduled to run 14 additional days of ^{87}Sr NMR experiments at 21.14 T in summer/fall 2005.

C.2.6 Column and Batch Studies

The formation of secondary mineral precipitates from reaction with tank wastes affects both contaminant removal and physical flow of contaminant waste streams. These effects were investigated in batch and flow-through column studies of pure quartz, a mixture of quartz and biotite, and Hanford sediment (Warden silt loam) contacted with STWL. Continuous Si dissolution and secondary mineral precipitation were the principal reactions observed. X-ray microtomography images of a reacted quartz column showed that secondary precipitates cemented quartz grains and modified pore geometry in the center of the column. Along the circumference of the packed column, however, quartz dissolution occurred continuously, suggesting that flow pathways can be altered by reaction with tank wastes. Batch experiments showed that the dominant secondary precipitates (nitrate-cancrinite) on the mineral surfaces after 3 to 10 d of reaction enhanced the sorption capacity of the sediment for ^{129}I(-I), ^{79}Se(VI), ^{99}Tc(VII), and ^{90}Sr(II). This study points out the importance of changes in mineralogy, both dissolution of primary phases and precipitation of secondary phases, in controlling contaminant uptake by changing sorption capacity and by changing porosity and flow paths that may influence subsequent reactions.

In a second study, a series of batch sorption and column experiments was conducted to investigate sorption and transport behavior of ^{99}Tc, ^{129}I, ^{79}Se, and ^{90}Sr on and through borehole sediments collected from the proposed low-level radioactive waste disposal facility at the Hanford Site (200 East Area). Experiments were done with Hanford sediment and uncontaminated Hanford groundwater, and simulated glass leachates (another alkaline waste stream that will occur at Hanford Site) spiked with individual radionuclides. Both test methodologies showed the strongest sorption occurred for ^{90}Sr, while ^{79}Se sorption was intermediate, and ^{129}I and ^{99}Tc showed the lowest sorption affinities on Hanford sediment among the radionuclides studied.

In a third study, a series of adsorption and desorption experiments were completed to determine the linearity and reversibility of iodide adsorption onto Hanford Site sediment. Adsorption experiments conducted with sediment and groundwater spiked with dissolved ^{125}I (as an analog tracer for ^{129}I) indicated that iodide adsorption was very low (K_d = 0.2 ml/g) at pH 7.5 and could be represented by a linear isotherm up to a total concentration of 100 mg/L. The results of desorption experiments revealed that up to 60 % of adsorbed I^- was readily desorbed after 14 d by iodide-free porewater. Because I^- is sorbed reversibly, it has a high mobility when uncontaminated porewaters contact the contaminated vadose sediments, making it one of the most problematic contaminants at the Hanford Site and thus a key element of the proposed work. Details on these three studies have been published recently (Um et al, 2004; Um et al., 2005, Um and Serne, 2005).

Publications resulting from this research are shown in **bold font** in the references section below. Several others are in preparation. Results from this work have also been presented in over 35 presentations by project personnel including national conferences (e.g., American Chemical Society, American Geophysical Union, Goldschmidt, Soil Science Society of America) and at invited academic seminars.

References (*publications resulting from current EMSP funding shown in bold*):

Bostick, B., A. Vairavamurthy, K. G. Karthikeyan and J. Chorover. 2002. Cesium adsorption on clay minerals: An EXAFS spectroscopic investigation. Environ. Sci. Technol. 36: 2670-2676.

Bowers, G. M. and K. T. Mueller. 2005. Electric field gradient distributions about strontium nuclei in tetrahedrally and octahedrally symmetric crystal systems. Physical Review B, in press.

Choi, S., M. K. Amistadi and J. Chorover. 2005a. Clay mineral weathering and contaminant dynamics in a caustic aqueous system. I. Wet Chemistry and Aging Effects. Geochim. Cosmochim. Acta. (in press).

Choi, S., G. Crosson, K. T. Mueller, S. Seraphin and J. Chorover. 2005b. Clay mineral weathering and contaminant dynamics in a caustic aqueous system. II. Mineral transformation and microscale partitioning. Geochim. Cosmochim. Acta. (in press).

Choi, S., P. A. O'Day, N. A. Rivera and J. Chorover. (submitted). Strontium incorporation in reaction products of kaolinite in simulated tank waste leachate from bulk and microfocused EXAFS analysis. Environ. Sci. Technol.

Chorover, J., S. Choi, M. K. Amistadi, K. G. Karthikeyan, G. Crosson and K. T. Mueller. 2003. Linking cesium and strontium uptake to kaolinite weathering in simulated tank waste leachate. Environ. Sci. Technol. 37: 2200-2208.

Chorover, J., P. A. Rotenberg, M. K. Amistadi, R. J. Serne, S. Choi and P. A. O'Day. (submitted). Reaction of cesium and strontium in Hanford sediments at high pH in synthetic tank waste leachate. Appl. Geochem.

Chorover, J., P. A. Rotenberg and R. J. Serne. 2004. Mineral formation and radionuclide sorption in waste-impacted Hanford sediments. *In* R. B. Wanty and R. R. Seal (eds.) *Water-Rock Interaction*. A. A. Balkema Publishers, Leiden. pp. 675-678.

Crosson, G. 2005. Quantitative and qualitative solid-state Nuclear Magnetic Resonance studies of hydroxide promoted dissolution of layered silicates. Department of Chemistry (Mueller-Major Advisor). Penn State University. Ph.D. Thesis.

Crosson, G., S. Choi, J. Chorover, P. A. O'Day and K. T. Mueller. (submitted). Solid-state NMR identification and quantification of newly-formed aluminum-containing phases in weathered kaolinite systems. Journal of Physical Chemistry B.

McKinley, J. P., C. J. Zeissler, J. M. Zachara, R. J. Serne, R. M. Lindstrom, H. T. Schaef and R. D. Orr. 2001. Distribution and retention of ^{137}Cs in sediments at the Hanford Site, Washington. Environmental Science & Technology. 35 (17): 3433-3441.

Um, W. and R. J. Serne. 2005. Sorption and transport behavior of radionuclides in the proposed low-level radioactive waste facility at the Hanford Site, Washington. Radiochim. Acta. 93: 57-63.

Um, W., R. J. Serne and K. M. Krupka. 2004. Linearity and reversibility of iodide adsorption on sediments from Hanford, Washington under water saturated conditions. Water Research. 38 (8): 2009-2016.

Um, W., R. J. Serne, S. B. Yabusaki and A. T. Owen. 2005. Enhanced radionuclide immobilization and flow path modifications by dissolution and secondary precipitates. J. Environ. Quality. 34 (in press).

Wan, J. M., T. K. Tokunaga, J. T. Larsen and R. J. Serne. 2004a. Geochemical evolution of highly alkaline and saline tank waste plumes during seepage through vadose zone sediments. Geochimica et Cosmochimica Acta. 68 (3): 491-502.

Zachara, J. M., S. C. Smith, C. X. Liu, J. P. McKinley, R. J. Serne and P. L. Gassman. 2002. Sorption of Cs^+ to micaceous subsurface sediments from the Hanford site, USA. Geochimica Et Cosmochimica Acta. 66 (2): 193-211.